proposed photodetector is shown to have the maximum responsivity of ~34 mA/W and external quantum efficiency (EQE) of ~8.8% over the specified visible range of 450-650 nm at -2V bias voltage.

**Chapter-3** reports an FTO/ZnO/$CH_3NH_3PbI_3$/MoOx/Ag structure based photodetector fabricated on FTO (Fluorine doped tin oxide) coated glass substrate. The hybrid perovskite $CH_3NH_3PbI_3$ is the active material, ZnO layer acts as the ETL, MoOx layer acts as the HTL and Ag is the contact electrode. The proposed device possess the maximum responsivity of ~21.8 A/W and EQE of ~6200% at ~ 436 nm near the blue light spectrum under a low reverse bias voltage of 1 V.

**Chapter-4** reports the fabrication and characterization of ITO/$BiFeO_3$ NPs/$CH_3NH_3PbI_3$/Ag based inorganic-organic heterojunction photodiode for operating in the visible-NIR (near-infrared) region. The photodetector shows the maximum responsivity of ~2 A/W, EQE of ~310% and detectivity of ~$7.8x10^{12}$ $cmHz^{1/2}/W$ at ~800 nm under -2 V bias voltage.

**Chapter-5** includes the major findings of the thesis along with a brief outline for the future scope of research related to the present thesis work.

----XXX----

# CHAPTER 1

## Introduction and Scope of the Thesis

Contents

# CHAPTER 1

# Introduction and Scope of the Thesis

## 1.1 Photodetector

Photodetector is a type of optoelectronic device which is used to measure optical radiation in the form of electrical current or voltage. It converts photon energy into electrical energy through the generation of extra electron-hole pairs in semiconductor materials used in the device. The photoelectric effect proposed by Albert Einstein in 1905 was a ground-breaking step for the development of photodetectors. According to the photoelectric effect, electrons ($e^-$) are emitted from the surface of a metal when photons with energy greater than the work function ($\Phi$) of the metal are incident on the metal's surface [1]. This observation is extended to semiconductors for developing optoelectronics devices. When photons with energy more than the bandgap energy of any semiconductor are incident on the semiconductor, electrons in the valence band (VB) of the semiconductor absorb the photons and are then excited from VB to the conduction band (CB) by leaving holes in the VB. As a result, excess electron-hole pairs (EHPs) are created in the semiconductor by the applied optical illumination. These EHPs are separated and drifted in opposite directions in a photodetector device by an electric field to result in an output electrical current of the device. The output current is proportional to the intensity of the incident illumination on the photodetectors. The working of the photodetectors is thus divided into three parts: (i) charge carrier generation by incident light, (ii) charge carrier transportation (including separation) by electric field, and (iii) extraction of carriers at the terminal to generate an output electrical signal.

Photodetectors are extensively used in optical communication and computing, remote sensing, environmental monitoring, night-time surveillance, image analyzing, and biological investigations [2]-[4]. The materials and device structures of various types of photodetectors largely depend on the type of applications. In general, direct bandgap semiconductors such as GaN, GaAs, InGaAs, and other III-V compound semiconductors are widely used materials for optoelectronic applications including photodetectors. However, the fabrication cost of these materials based photodetectors is very high due to the requirement of very expensive and sophisticated equipments like liquid phase epitaxy (LPE), molecular beam epitaxy (MBE) etc [4]. That is why low-cost solution processing based on organic and inorganic thin-film based photodetectors have drawn considerable attention in recent times [5]. The material processing and fabrication of such devices can be done at the low-cost room/low-temperature solution methods without requiring any sophisticated analytical equipments. In the last decade, perovskites have been projected as important materials for photodetection applications [6]-[8] due to their direct bandgap nature, high optical absorption coefficients, large exciton diffusion length, high dielectric constant, low binding energy, high drift velocity, long carrier lifetime and wide range of optical bandgaps. Perovskites are naturally occurring minerals with a generalized chemical formula of $ABX_3$ (e. g. $CaTiO_3$) where A and B are metal cations and X is an anion. The first perovskite $CaTiO_3$ was discovered by German mineralogist Gustav Rose in 1839 and the class of $ABX_3$ materials were named *perovskites* in honour of the Russian mineralogist Lev Perovski [9]. These materials are inorganic in nature. Recently, a hybrid form of organic-inorganic perovskites with a generalized formula of $ABX_3$ using A as a methylammonium cation (e. g. $CH_3NH_3^+$), B is a divalent metal cation (e. g. $Pb^{2+}$, $Sn^{2+}$, $Cd^{2+}$, etc.) and X is a halide ion (e. g. $Cl^-$, $Br^-$, or $I^-$) have shown great potentials for photovoltaic applications [7]. However, these materials have been less explored for the

designing of photodetector devices. In view of the above, the objective of the present thesis is to explore both the inorganic and organic perovskites for the fabrication of some photodetectors fabricated by low-cost solution methods.

### 1.1.1 Device Structures for Photodetectors

Photodetectors are fabricated either in a horizontal or vertical structure. The schematic representations of the photodetector with horizontal and vertical structures are shown in Figure 1.1. Photoconductors and phototransistors are examples of horizontal structures, whereas photodiodes (p-n junction, Schottky junction, and heterojunction devices) are of vertical structures [10].

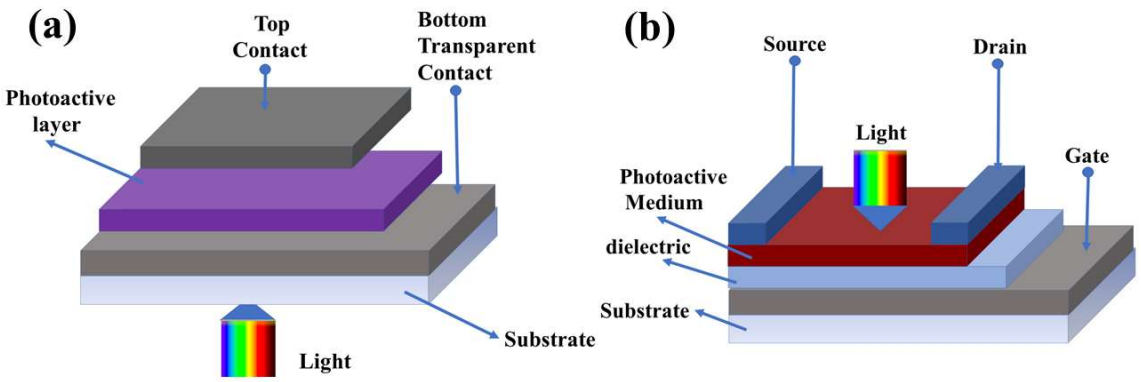


**Figure 1.1:** The diagrammatic representation of the photodetector in (a) vertical structure and (b) horizontal structure.

All the photoconductors and photodiodes are two-terminal devices with anode and cathode electrodes, while phototransistors are three-terminal devices with source, drain, and gate electrodes [11]. Different types of photodetectors are discussed in the following subsections.

#### *1.1.1.1 Photoconductors*

Photoconductors, also called photoresistors or light-dependent resistors, are the most basic form of two-terminal devices where the incident light is used to generate extra

electron-hole pairs to change the conductivity of a photoactive semiconductor by the photoelectric effect. The photoconductor device has two ohmic contacts on the semiconductor surface as shown in Figure 1.2. The photo-induced electron-hole pairs change the conductivity of semiconductor material leading to the enhanced current in the photodetector.

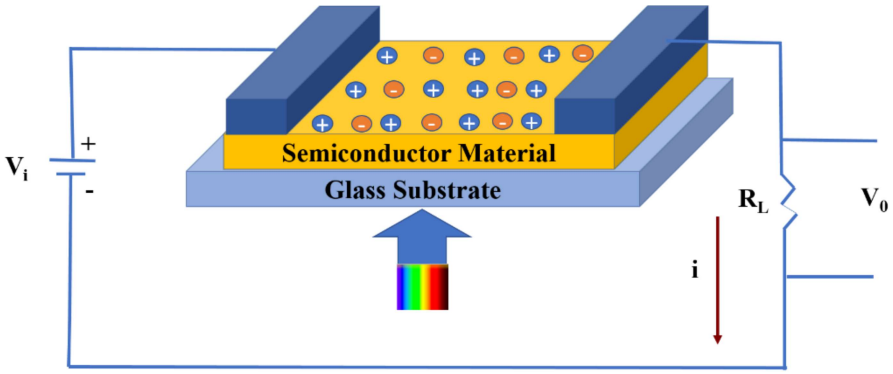


**Figure 1.2:** The schematic diagram of the photoconductor device.

### *1.1.1.2 Photodiodes*

The photodiode, in the simple sense, is a p-n junction diode operated under reverse bias with an illumination incident on it. The schematic structure of the photodiode is shown in Figure 1.3. For $p^+n$ junction, the depletion region width (W) formed under a reverse bias voltage of $V_R$ at the p-n junction is given by [12]:

$$W = \sqrt{\frac{2\varepsilon(V_{bi} + V_R)}{qN_d}} \qquad \ldots\ldots\ldots\ldots (1.1)$$

where ε, q and $N_d$ represent the effective dielectric constant, electronic charge, and donor concentration, respectively, and $V_{bi}$ is the built-in potential developed across the depletion region at the thermal equilibrium of the junction.

The energy band diagram for the charge transport under light illumination is illustrated in Figure 1.4. When illumination is applied to the device, electrons are excited from the valence band to the conduction band thereby creating excess electron-hole pairs (EHPs) in the semiconductors. Under the reverse bias operation, the electric field in the

depletion region is large enough to separate the photogenerated electrons and holes by drifting them in the opposite directions. Electrons are drifted in the opposite direction of the field while the holes are drifted in the same direction of the electric field in the depletion region. These electrons and holes are collected by the respective electrodes to obtain a photocurrent (proportional to the incident illumination) as the output of the photodiodes.

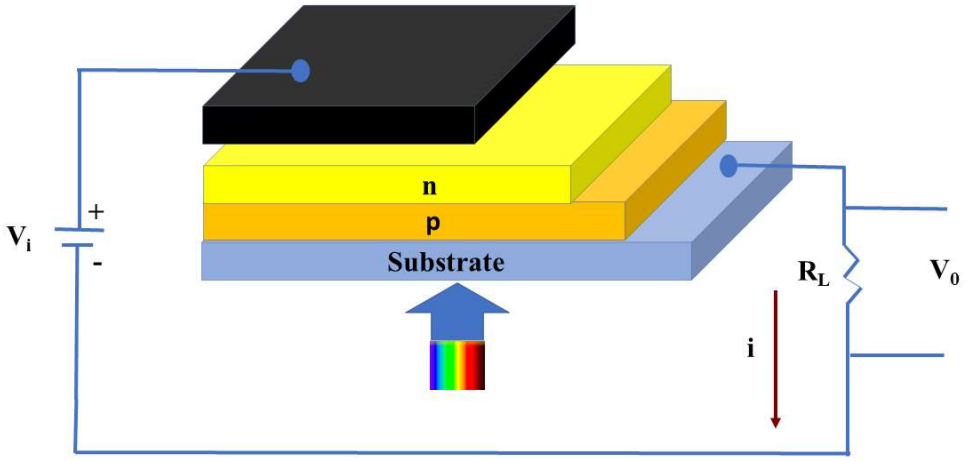


**Figure 1.3:** The schematic diagram of the p-n photodiode device.

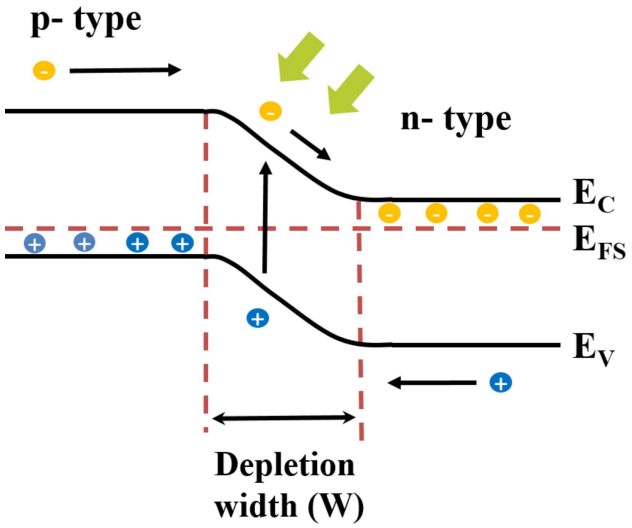


**Figure 1.4:** Representation of the energy band diagram for the p-n photodiode device.

Photodiodes may be of homojunction and heterojunction types. When p-type and n-type regions of the photodiodes are of the same semiconductor, we call a homojunction

while the heterojunction photodiodes are formed by the junction of two different semiconductors. The light may be coupled into the device through a transparent substrate of the device as shown in Figure 1.3.

Various other device structures namely the p-i-n photodiode [7], avalanche photodiode [13] and Schottky junction photodiode [14] are also used for photodetection applications. The p-i-n diode structure is obtained by sandwiching an intrinsic semiconductor layer in between the p and n layers. The doping concentration of the p and n regions are maintained to make the intrinsic or lightly doped semiconductor region depleted under thermal equilibrium conditions so that the depletion width is nearly the same as the length of the intrinsic (i) region. The avalanche multiplication mechanism is explored in the avalanche photodiodes. The Schottky photodiodes are simply Schottky junction diodes illuminated through a transparent thin metal electrode used the Schottky contact on a semiconductor.

### 1.1.2 Key Performance Parameters of Photodetectors

The performance of the photodetectors is primarily evaluated by current-voltage *(I-V)* characteristics measured under dark and illuminated conditions of the device. The photocurrent is obtained by subtracting the dark current from the current under the measured illumination of the device. For any good photodetector, the dark current should be very small as compared to the current measured under illuminated conditions. Thus, the current under illumination is approximately equal to the photocurrent of good photodetectors. The *I-V* characteristics are used to extract the important performance parameters namely the *Responsivity* ($R_\lambda$), *External quantum efficiency* (EQE), *Detectivity* (D), and *Response Time* as briefly defined in the following.

### *1.1.2.1 Responsivity ($R_\lambda$)*

The responsivity of the photodetector expressed usually in A/W, is defined as the ratio of the generated photocurrent to the incident optical power at a wavelength (λ). Responsivity can be measured using the following equation [15]:

$$(R_\lambda) = \frac{I_{light} - I_{dark}}{P_d} \quad \text{..... (1.2)}$$

where $I_{light}$ is the current under illumination, $I_{dark}$ is the current under dark conditions. $I_{light}$ - $I_{dark}$ is the photocurrent and $P_d$ is the optical power, respectively.

Since responsivity ($R_\lambda$) is directly proportional to the quantum yield of a photodetector device, it should be very high for a high conversion rate from photon to electron-hole pairs in the active layer of the device.

### *1.1.2.2 Detectivity (D)*

The detectivity (D) of the photodetector represents the minimum optical power required to produce a measurable photocurrent of the device. Detectivity can be calculated using the following equation [16]:

$$D = R_\lambda * \sqrt{\frac{RA}{4kT}} \quad \text{..... (1.3)}$$

where k is the Boltzmann constant, *T* is the temperature, and *RA* is the resistance–area product which is defined as [16]:

$$RA = (\frac{dJ}{dV})^{-1} \quad \text{..... (1.4)}$$

where "*J*" is the photocurrent density of the photodetector.

### *1.1.2.3 External Quantum Efficiency (EQE)*

The external quantum efficiency (EQE) of the photodetector is an important parameter of any photodetector. The EQE is the ratio of the number of charge carriers collected by the electrodes of the photodetector to the number of photons of a given

energy (or wavelength) incident on the photodetector device from outside (i. e. incident photons). The EQE is determined by the given equation [17]:

$$EQE(\%) = \left(\frac{1240 * R_\lambda}{\lambda}\right) * 100 \qquad \ldots\ldots\ldots\ldots\ldots\ldots (1.5)$$

where $R_\lambda$ is the responsivity of the photodetector, λ is the wavelength of the incident light expressed in nm.

*1.1.2.4 Response Time*

The speed of operation of the photodetector is expressed in terms of the rise time ($\tau_r$) and fall time ($\tau_F$) of the output photocurrent when the device is exposed to a pulsed light. The rise time ($\tau_r$) is defined as the time required to change the output value from 10% to 90% of the steady output. Similarly, the fall time ($\tau_F$) is measured as the time required to decay from 90% to 10% of the falling edge of the photocurrent. Smaller values of the rise time and fall time are desirable for high-speed photodetector.

*1.1.2.5 Other Figure of Merits*

- *Noise equivalent power* (NEP): The NEP of the photodetector is defined as the lowest signal power to result in a signal-to-noise ratio (SNR) of one, when the electrical bandwidth of noise measurement is 1 Hz. The NEP is equal to the ratio of the output noise (amplitude) spectral density, say $N_o(f)$ expressed $\frac{A}{\sqrt{Hz}}$, to the responsivity (R) of the photodetector expressed as [6]:

  $$NEP = N(f)/R \qquad \ldots\ldots\ldots\ldots\ldots\ldots (1.6)$$

  The unit of the NEP is thus $Watt/\sqrt{Hz}$.

- *Linear dynamic range* (LDR): The LDR of a photodetector is defined as the range of light intensity over which the photocurrent response is linearly

proportional to the incident illumination intensity on the photodetector. The LDR is expressed in dB is given by [18]:

$$LDR = 20\ Log\frac{P_{max}}{P_{min}} \quad \text{..... (1.7)}$$

where $P_{min}$ and $P_{max}$ are the minimum and maximum incident optical power over which the photocurrent shows a linear relationship with the incident power.

## 1.2 Perovskite Materials for Photodetectors

As introduced earlier, the perovskites belong to a class of materials with common formula of $ABO_3$ which are similar to the calcium titanium ($CaTiO_3$) with A and B are two metal ions. The $ABO_3$ formula based inorganic perovskites have drawn considerable attention due to their high permittivity, ferroelectricity and piezoelectricity properties [19]. Another class of perovskites of general formula $ABX_3$, known as halide perovskites, was obtained by replacing "O" in $ABO_3$ by a halide ion "X" (e. g. $Cl^-$, $Br^-$, or $I^-$). The cesium lead halides ($CsPbX_3$) are the first halide perovskites discovered by Wells in 1893 [20]. C. K. Moller suggested the generalized formula $ABX_3$ of the halide perovskite structures in 1957 [21]. In 1978, D. Weber replaced Cesium in $CsPbX_3$ by methylammonium cation (MA = $CH_3NH_3^+$) to achieve a new class of organic-inorganic halide perovskite materials [22], [23]. Among various halide perovskites, the hybrid perovskite methylammonium lead iodide ($CH_3NH_3PbI_3$) is the most commonly used hybrid halide perovskite as photoactive material in photodetection applications. The generalized crystal structure of the halide perovskites is shown in Figure 1.5.

Perovskites are also classified into zero-dimensional (0-D) perovskites with crystal structure of $A_4BX_6$, one-dimensional (1-D) perovskites with the crystal structure

of $A_6BX_5$, two-dimensional perovskites with the crystal structure of $A_2BX_4$, and three-dimensional (3-D) perovskites with the structure of $ABX_3$ [24]. These halide perovskites have drawn remarkable attention for solar cell and light-emitting diode applications owing to their important properties such as high absorption coefficient, high charge carrier mobility, high emission efficiency, tunable wavelength, and low defect densities [25]. However, the commercialization of halide perovskite devices is restricted by mainly two major drawbacks namely the poor stability and high toxicity (due to the presence of $Pb^{2+}$) of the halide perovskite materials.

In the present thesis, we have attempted to explore $BiFeO_3$ and $CH_3NH_3PbI_3$ perovskites for photodetection applications. Here $BiFeO_3$ is an inorganic perovskite while $CH_3NH_3PbI_3$ is a hybrid halide perovskite. The following subsections are devoted to outline some important properties of these materials for photodetector device applications.

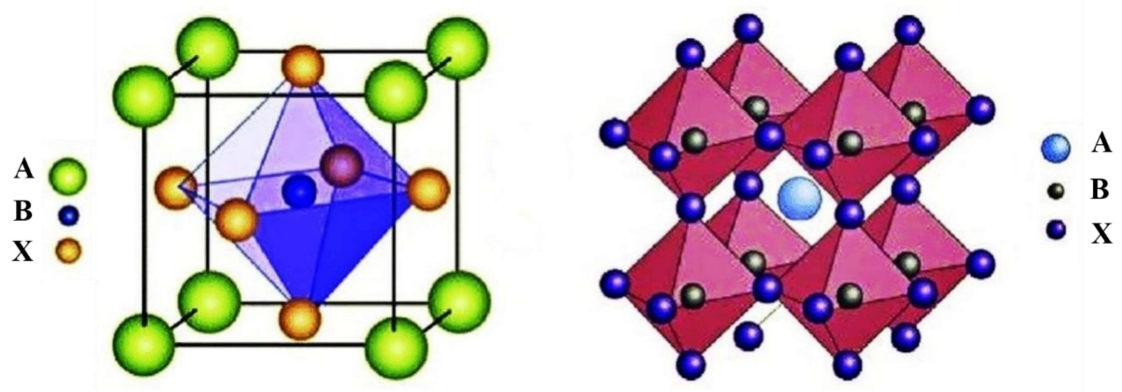


**Figure 1.5:** Unit cell of the perovskite crystal structure.

### 1.2.1 Properties of $BiFeO_3$ Inorganic Perovskite

We have already discussed in Sec 1.1 that an electric field is required to drift the electrons and holes of the photo-generated electron-hole pairs (EHPs) in the opposite directions to result in a photocurrent in the photodetector. For a p-n junction photodetector, the electric field in the depletion plays a significant role in separating the

electrons and holes of the photo-generated EHPs. Interestingly, when a light is incident on the $BiFeO_3$ inorganic ferroelectric perovskite material, the separation of photo-generated electrons and holes may take place within the material itself due to the presence of an internal electric field created by ferroelectric polarization [26]. The presence of non-centro symmetry or breaking of strong inversion symmetry of ferroelectric perovskites may produce a large field in this material [27]. Thus, $BiFeO_3$ material is a good candidate for photodetector applications with a wide range of absorption spectrum over 300-800 nm [27], [28]. In addition to the above, $BiFeO_3$ has also other important properties such as good chemical stability, a wide range of bandgap, eco-friendly and switchable rectifying behaviour. $BiFeO_3$ is widely used for photovoltaic devices, photodetectors and memory elements due to its aforementioned promising electronic and optoelectronic properties [26]-[32].

### 1.2.2 Properties of $CH_3NH_3PbI_3$ Hybrid Perovskite

The bandgap and hence the optical absorption properties of the hybrid $CH_3NH_3PbX_3$ ($X = Cl^-$, $Br^-$, or $I^-$) perovskite materials can be varied by selecting different halide anions ($X = Cl^-$, $Br^-$, or $I^-$). Tunable bandgap based hybrid perovskites can be achieved by developing the mixed hybrid halide solid solutions [33], [34].

Among various hybrid halide perovskites, the methylammonium lead iodide ($CH_3NH_3PbI_3$) is the most widely used hybrid perovskite for optoelectronic applications due to its unique intrinsic semiconducting property, high mobility of photogenerated carriers, high absorption coefficient, modest bandgap properties, excellent solubility, long carrier lifetimes, and low-cost low-temperature processing [35], [36]. It acts as a strong sensitizer to light over 300-800 nm wavelengths [37]. Nowadays, $CH_3NH_3PbI_3$ is used for colour image sensing in a digital camera, optical communication, and medical

diagnostics [38]. The material has an exciton diffusion length of ~100 nm with a very low defect density which produces a low saturation current in heterostructure devices [39], [40].

## 1.3 Fabrication Process for Perovskite Photodetectors

The perovskite photodetectors can be of a single layer or multiple layers of different perovskite materials [7], [14]. In general, multilayer-photodetectors are more efficient than single layer due to increased absorption and improved charge carrier separation at the interfaces. The multi-layered photodetectors include mainly three layers: the electron transport layer (ETL), photoactive layer and hole transport layer (HTL). The schematic structure of the perovskite (p-i-n) photodetector is shown in Figure 1.6. Appropriate metal electrode contacts are required on the ETL and HTL to act as cathode and anode respectively. Every layer of the device plays important role in deciding the performance of the photodetectors. The photoactive layer is the heart of the photodetectors where light to be detected is mainly allowed to be absorbed to generate excess electron-hole pairs to contribute to the photocurrent of the device. The main task of the charge transport layers ETL and HTL is to collect photogenerated electrons and holes in the active layer efficiently so that an optimum photocurrent can be obtained as the output of the photodetectors. The fabrication of the photoactive layer, charge transport layers and contact electrodes are discussed briefly in the following subsections.

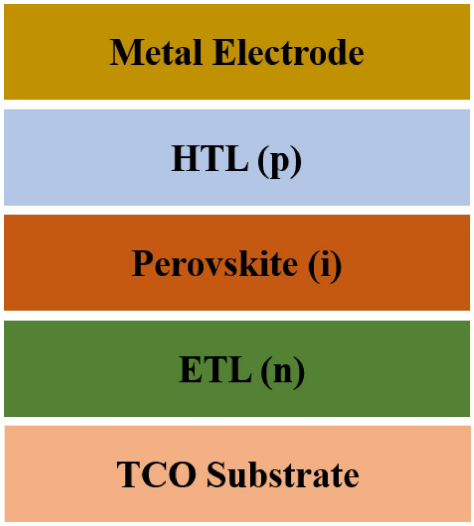


**Figure 1.6:** The schematic structure of (p-i-n) perovskite photodetector.

### 1.3.1 Fabrication of Photoactive Layer

In this thesis work, inorganic perovskite $BiFeO_3$ and hybrid perovskite $CH_3NH_3PbI_3$ are used as photoactive layers. The conduction band and valence band energy positions in the inorganic material $BiFeO_3$, while the LUMO and HOMO labels in the organic perovskite material $CH_3NH_3PbI_3$ can easily be modified by changing the anions. The thin film deposition techniques play significant roles in the fabrication of perovskite materials based electronic devices. In general, the inorganic perovskite materials (e. g. $BiFeO_3$) are synthesized using the solid-state route [41], [42] while the hybrid perovskite materials (e. g. $CH_3NH_3PbI_3$) are synthesized by the solution method [43], [44]. Inorganic perovskite materials are soluble in several polar protic solvents such as the methanol ($CH_3OH$) and ethanol ($C_2H_5OH$) [27], [29] while the hybrid perovskite materials are soluble in dipolar aprotic solvents such as the dimethylformamide ($C_3H_7NO$) and dimethyl sulfoxide ($C_2H_6OS$) [8], [14]. The thin films of inorganic/hybrid perovskite materials can be deposited on the substrates at room temperatures using solution processing techniques. In this method, a homogeneous solution of inorganic/hybrid perovskite material is first

obtained by dissolving it in a suitable solvent. Various deposition procedures, such as drop casting, spin coating, and dip coating, are used to deposit the resulting solution on the substrate in the form of thin films. Spin coating is regarded as one of the most effective deposition processes for producing a smooth thin layer with acceptable surface morphology. Deposition of spin coatings is also a cost-effective method. In this thesis work, the thin films of inorganic/hybrid perovskite materials are deposited using the spin coating technique.

The sol-gel based thin film preparation techniques are demonstrated in Figure 1.7. The entire process may be divided into two parts: sol-gel preparation and thin film deposition. The sol-gel process involves the formation of colloidal particles of the desired perovskite in the *sol*, gelation of the sol by the agglomeration of these particles or sub-units into a big gel network structure, removal of the solvent and heat treatment to transfer gel into solid [45], [46]. Depending on reaction conditions, the sol particles may grow further or form a gel as shown in Figure 1.7. The sol-gel solution of the precursor is then used for thin-film preparation by dipping a substrate into the solution (i. e. dip-coating) or spreading the solution over the surface of a substrate (on which the film is to be grown) using a spin coater. In this thesis, spin-coating has been used for the perovskite film deposition.

In the spin-coating method, the sol-gel solution is dropped on the desired substrate using a micro dropper and then the substrate is rotated at a certain speed using a photoresist spinner as demonstrated in Figure 1.8. The step may be followed multiple times to achieve a multi-layered perovskite film of desired thickness. The TSE-system GmbH (model SPM-150LC, Germany) spin-coater was used for the fabrication of inorganic/hybrid perovskite films in the present thesis.

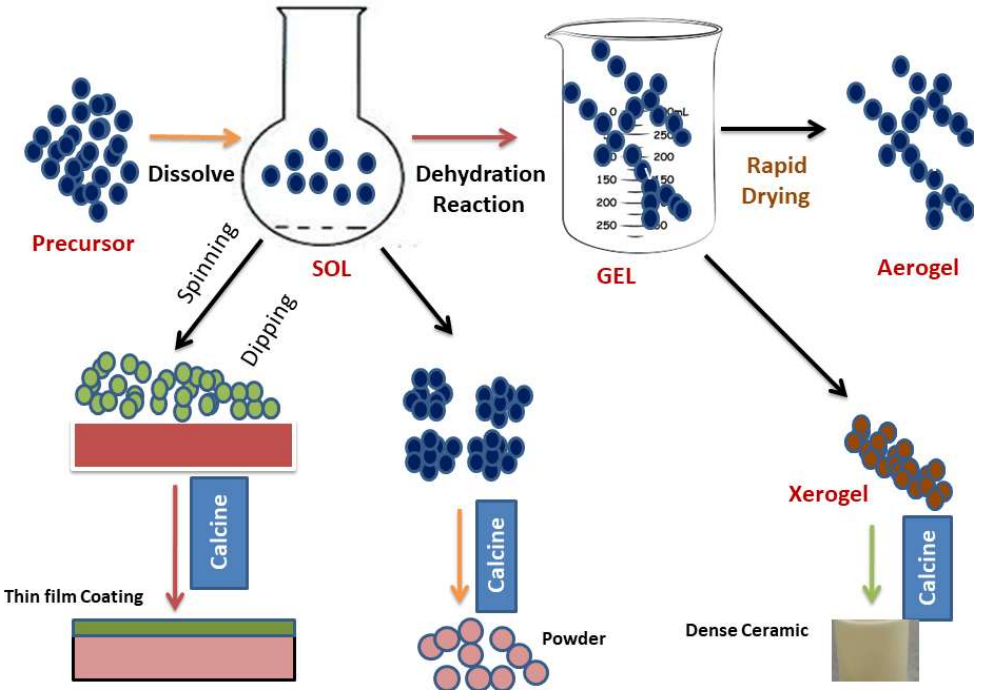


**Figure 1.7:** The schematic diagram of the sol-gel formation mechanism.

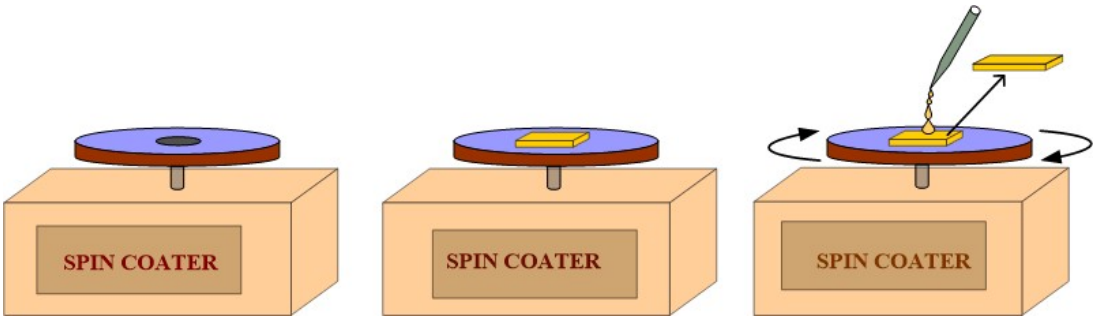


**Figure 1.8:** Spin-coating process steps (a) Spin-coating unit (b) Substrate on the spin-coating unit and (c) film deposition on the substrate.

### 1.3.2 Charge Transport Layers (ETL and HTL)

Charge transport layers ETL and HTL play significant roles in the effective collection of the photogenerated electrons and holes by minimizing their recombination in the active region of the photodetectors. Suitable materials need to be carefully chosen for the ETL and HTL so that the minimum absorption of the light can take place in these layers and the maximum light can be absorbed in the photoactive layer. Proper energy band

alignments among the ETL, active region and HTL layers should be there to minimize the recombination of the photogenerated excess carriers in the active layer. The ETL is used to block the injection of holes while the HTL prevents the electron injection from the external power supply into the active layer to reduce the recombination of photogenerated charge carriers in the photoactive region. When the photodetectors are operated under reverse operation, the ETL (HTL) layer extract the photogenerated electrons (holes) generated in an active region and transport them to its electrode contact. The ETL and HTL thus enhance the efficiency of the photodetectors and solar cells. In general, wide bandgap materials are used for the HTL and ETL in broadband photodetectors [47], [48]. In the present thesis work, the thin films for the ETL and HTL are deposited using the spin coating method and thermal evaporation unit (Model No. FL400, SMART COAT 3.0 A, Hind High Vacuum India), respectively.

### 1.3.3 Fabrication of Contact Electrodes

The suitable cathode and anode metal electrodes are required to be fabricated on the ETL and HTL for the effective collection of electrons and holes transported through the ETL and HTL under revise bias operation of the photodetectors, respectively. Various physical vapour deposition methods like a thermal deposition, electron beam evaporation, and sputtering techniques are used for the metal electrode depositions. The thermal evaporation unit (Model No. FL400, SMART COAT 3.0 A, Hind High Vacuum India) has been used for the metal (Au, Ag, and Al) electrode contact fabrication in the present thesis work. The schematic of the thermal evaporation unit used in the thesis is shown in Figure 1.9.


**Figure 1.9:** Thermal evaporation deposition instrument for metal electrode deposition.

## 1.4 Characterization Techniques for Perovskite Based Photodetectors

Inorganic/hybrid perovskite material thin films were characterized for their various properties such as crystal structures, surface morphology, absorbance characteristics, photoluminescence (PL), etc. The characterization techniques used in the present work are briefly presented in the given below section.

### 1.4.1 Material Characterization Techniques

The structural, electrical and optical characterization of the synthesized perovskites and their thin films used in the thesis are characterized using the following techniques:

#### *1.4.1.1 X-Ray Diffraction (XRD)*

A new technique for the material characterizations at the atomic scale was feasible with the discovery of X-rays in 1885. X-ray diffraction (XRD) is a powerful characterization tool applicable for thin films, powders and crystals to investigate the lattice parameters, crystal structure, defects, and stress in the materials. In 1913, W. H. Bragg and W. L. Bragg explained the formation of diffraction patterns using the famous equation known as Bragg's law [49].

$$2d\ Sin\theta = n\lambda \quad \text{..... (1.8)}$$

where $\theta$ is the angle of incidence of the X-rays of wavelength λ on the material, and $n$ is an integer representing the order of reflection and '$d$' represents the lattice spacing in-between two planes.

If the XRD curve only has one peak, the material is likely single crystalline. Multiple peaks, on the other hand, indicate that the material is polycrystalline. The material is deemed amorphous if there is no peak in the XRD Spectra. The operation and working principle of XRD is illustrated in Figure 1.10. In the present thesis work, the XRD analyses of the inorganic/hybrid perovskite materials and various their thin films were performed using the XRD unit Rigaku procured from Japan.

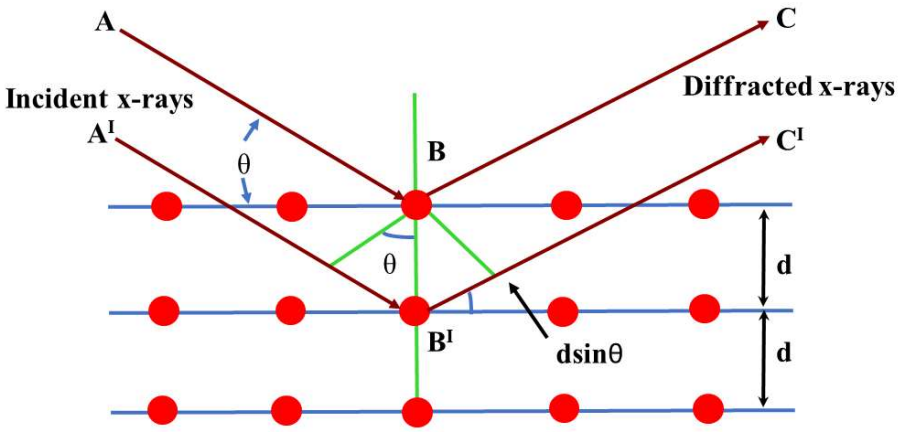


**Figure 1.10:** Working principle of X-ray diffraction (XRD).

### *1.4.1.2 Scanning Electron Microscopy (SEM)*

Scanning electron microscopy (SEM) is a strong microscopic technique for studying thin film morphology, topography, and surface characteristics. A scanning electron microscope (SEM) image of a sample's surface is created by scanning the surface with a concentrated electron beam of high energy electrons. The beam's high-energy electrons interact with the sample's surface to produce a variety of signals, which are then analysed to extract surface features such as topography, morphology, and composition [50], [51]. The electron beam excites the atoms in the sample, causing a significant number of secondary electrons to be emitted from the excited atoms. The secondary electrons released by the atoms are gathered using a specific detector, resulting in the formation of displaying the topological picture of the surface of the sample. The electron beam is scanned in a raster scan pattern. The beam scanning is combined with the detector signal to produce an image of high resolution (HR) [52]. The operation and working principle of SEM is illustrated in Figure 1.11. In the present thesis work, the high-resolution SEM (HRSEM) images of various thin films under study were obtained using Carl Zeiss Microscopy Ltd. (model EVO MA 15/18), UK.

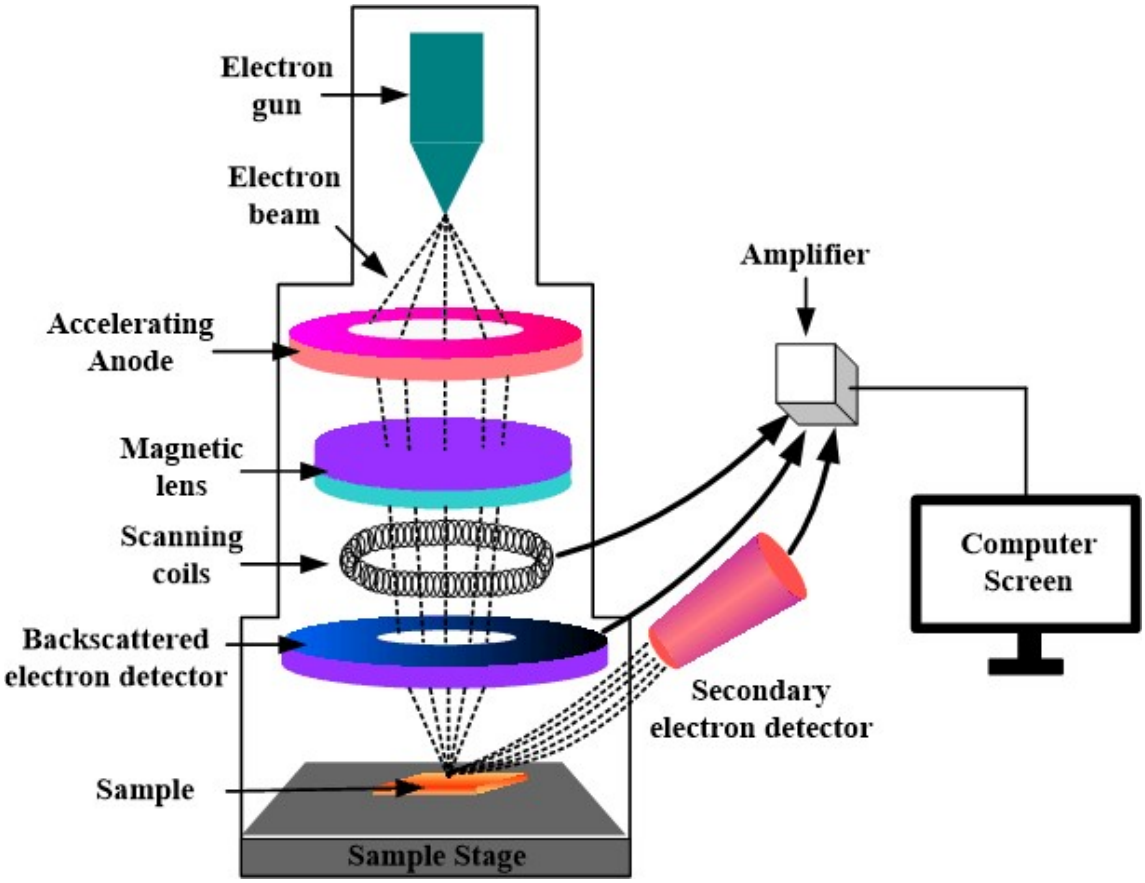


**Figure 1.11:** Experimental measurement setup and working of the SEM instrument.

### *1.4.1.3 UV-Visible Spectroscopy (UV-Vis)*

Ultraviolet-Visible (UV-Vis) spectroscopy is a powerful technique to analyse the optical properties of the materials. It measures the absorbance characteristics from transmittance ($T$) characteristics as $A = -\log(T)$. The obtained absorbance spectrum can be used to match the identification of the functional group of materials. It is also used to measure the optical bandgap of the material using tauc plot relationship as given below [53]:

$$\alpha = \beta \frac{(h\nu - E_g)^{n/2}}{h\nu} \quad \ldots\ldots\ldots\ldots\ldots (1.9)$$

where n is an integer and depends on whether the bandgap is direct (n =1) or indirect (n = 4), $\alpha$, $h$, $\nu$, $E_g$ and $\beta$ are the absorption coefficients, Plank's constant, light frequency, bandgap and an arbitrary constant, respectively. The extrapolation of the linear graph yielded an intercept on $h\nu$ axis that corresponds to energy equivalent to the bandgap energy. The schematic diagram of a UV-Vis spectroscopy is displayed in Figure 1.12. UV-Vis spectroscopy (V-770 from JASCO, Japan) has been used for the thin film characterization in the present thesis work.

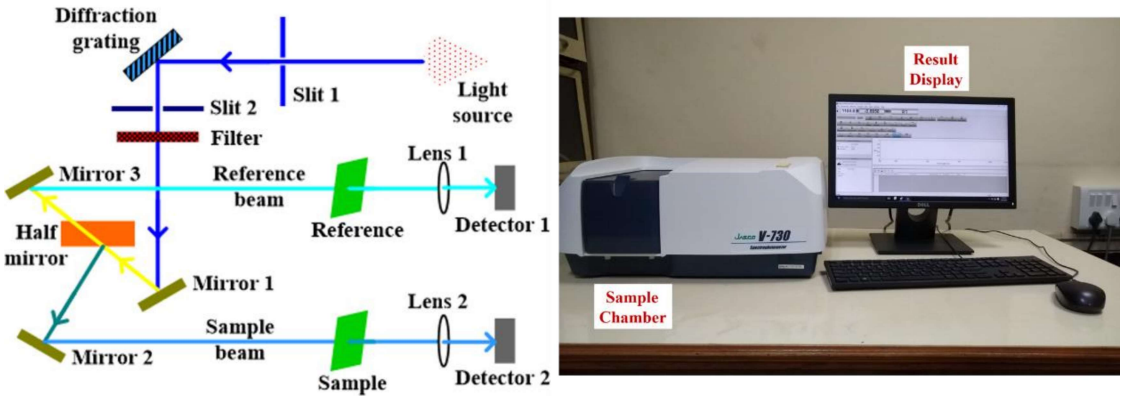


**Figure 1.12:** Working principle and experimental measurement setup for the UV-Vis spectroscopy.

### *1.4.1.4 Photoluminescence Spectroscopy (PL)*

The PL spectroscopy is used to analyse various information of material such as material defects, impurity levels, bandgap determination, charge carrier recombination rate etc. in a non-contact and non-destructive type manner [51]. Through a monochromator, visible light and neighbouring light are incident on the sample under investigation to excite the material to a higher electronic state by photo-excitation. Following relaxation, the excited electrons return to lower energy levels, resulting in photoluminescence (PL). The energy of the emitted photons (i.e. photoluminescence) is determined the energy difference between the excited state and the equilibrium state of the material. The schematic representation for the photoluminescence spectroscopy technique is shown in Figure 1.13. In the present thesis work, the PL measurements of

various samples were performed using the spectrometer (FLS 980) from Edinburgh Instruments, UK.

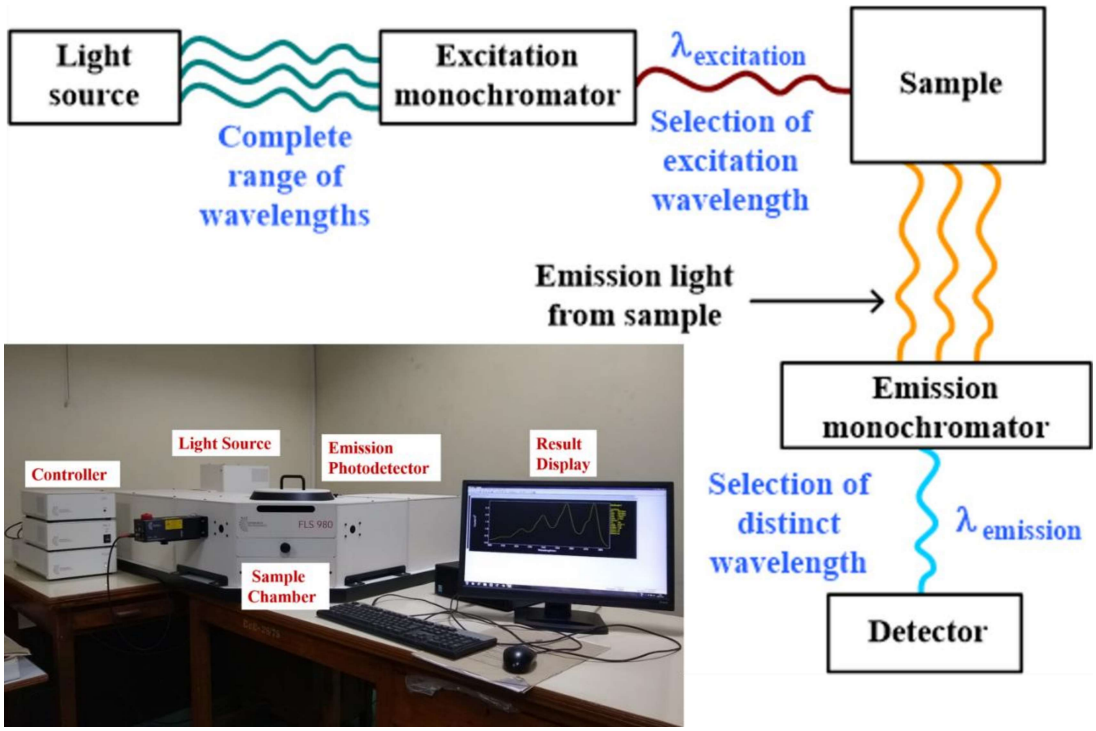


**Figure 1.13:** Experimental Setup and working principle of the Photoluminescence spectroscopy.

### 1.4.2 Device Characterization Techniques

The fabricated perovskite based photodetectors are characterized for determining their various performance parameters. Various measurement techniques used for the perovskite based photodetectors in the present thesis are discussed in the following.

#### *1.4.2.1 Dark Conditions Measurements*

Like other semiconductor devices, the electrical characteristics of the inorganic/hybrid perovskite materials based devices were done using a semiconductor parameter analyser (SPA) (Make: Keysight, Model: B1500A) with 2 source measuring units (SMUs). The SPA is used to measure the current-voltage (*I-V*) characteristics of the fabricated photodetector devices under dark and illuminated conditions. The SPA is also

used for capacitance-voltage (*C-V*) characteristics of the fabricated devices under study in the present thesis. The measurement setup for the electrical characterization of the inorganic/hybrid perovskite materials based devices using SPA is shown in Figure 1.14-1.15.

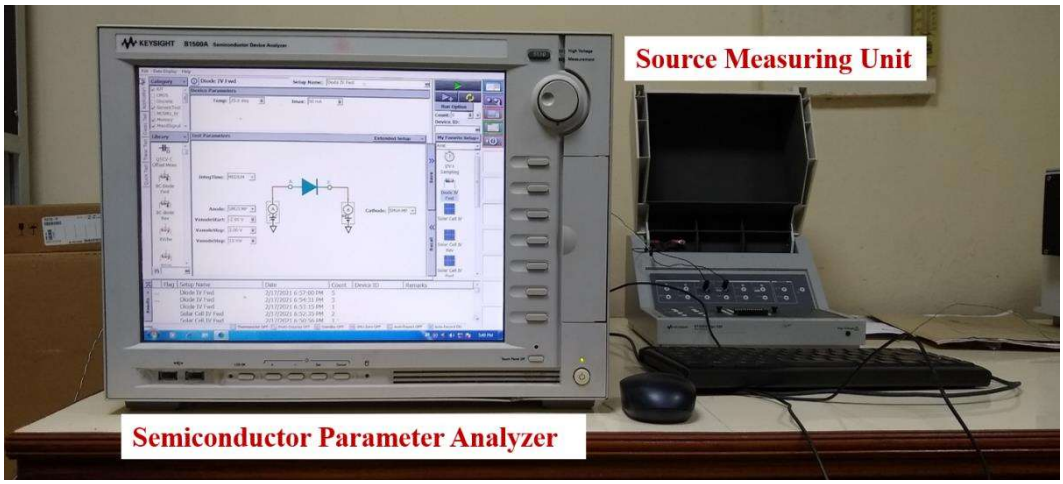


**Figure 1.14:** Semiconductor parameter analyser for the measurements of various electrical parameters.

*Current-Voltage (I-V) characteristics*: I-V characteristics of the photodetectors under dark and illumination are used for the photocurrent measurement of the devices under reverse bias operation.

*Capacitance-Voltage (C-V) characteristics*: The C-V plots give information about the variation in the junction capacitance of a diode with the change in the sweeping voltage applied across the terminals of the device. The (*C-V)* characteristics of any diode depend on its junction properties. The measured (*C-V*) characteristics can also be used to extract the carrier concentration, depletion width and barrier height of p-n junction diodes [50].

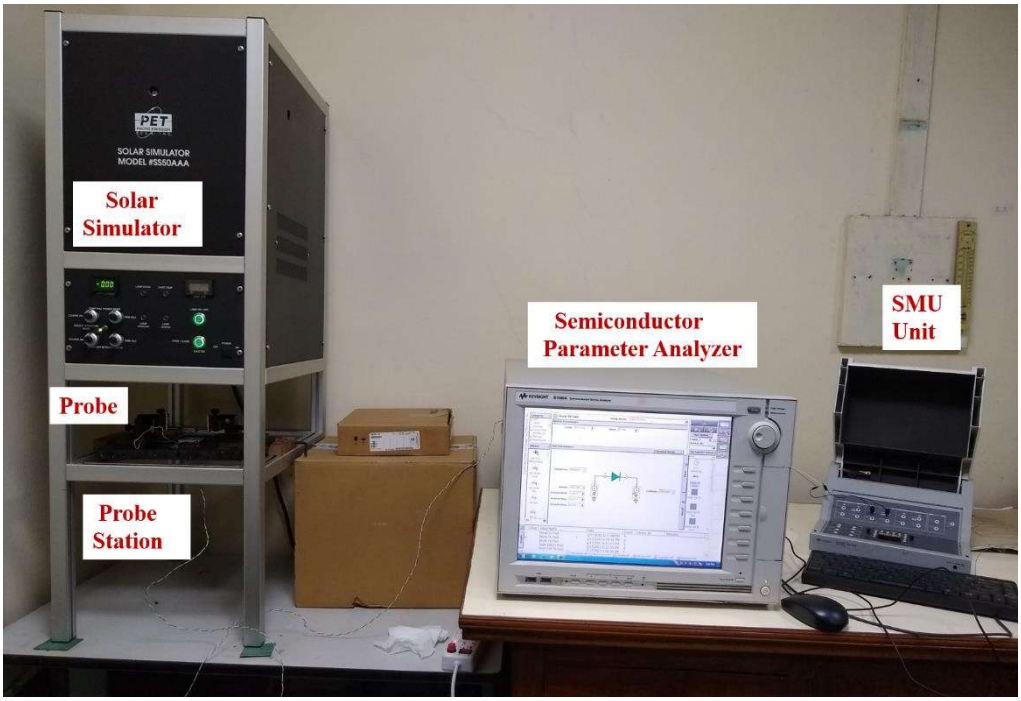


**Figure 1.15:** Experimental measurement setup for the electrical characterizations.

### *1.4.2.2 Photoresponse Measurements*

The difference between the currents under illumination and dark conditions gives the photocurrent of the photodetectors. The I-V measurements under illumination are used to obtain various performance parameters, such as the responsivity, external quantum efficiency (EQE) and detectivity of the photodetectors.

*Photocurrent-Wavelength Characteristics*: I-V characteristics measured under illumination for different incident wavelengths are used to obtain the photocurrent-wavelength characteristics of the photodetectors. This is used to plot the responsivity, detectivity and EQE as functions of applied wavelengths of the incident light to the detectors. In the present thesis, measurements have been carried for lights with wavelengths in the ultraviolet (UV), visible, or infrared (IR) regions. The wavelength of monochromatic light is varied over a specified range and the photocurrent is recorded for

every incident wavelength of light. The complete experimental instrumental setup for photocurrent versus wavelength measurements is shown in Figure 1.16.

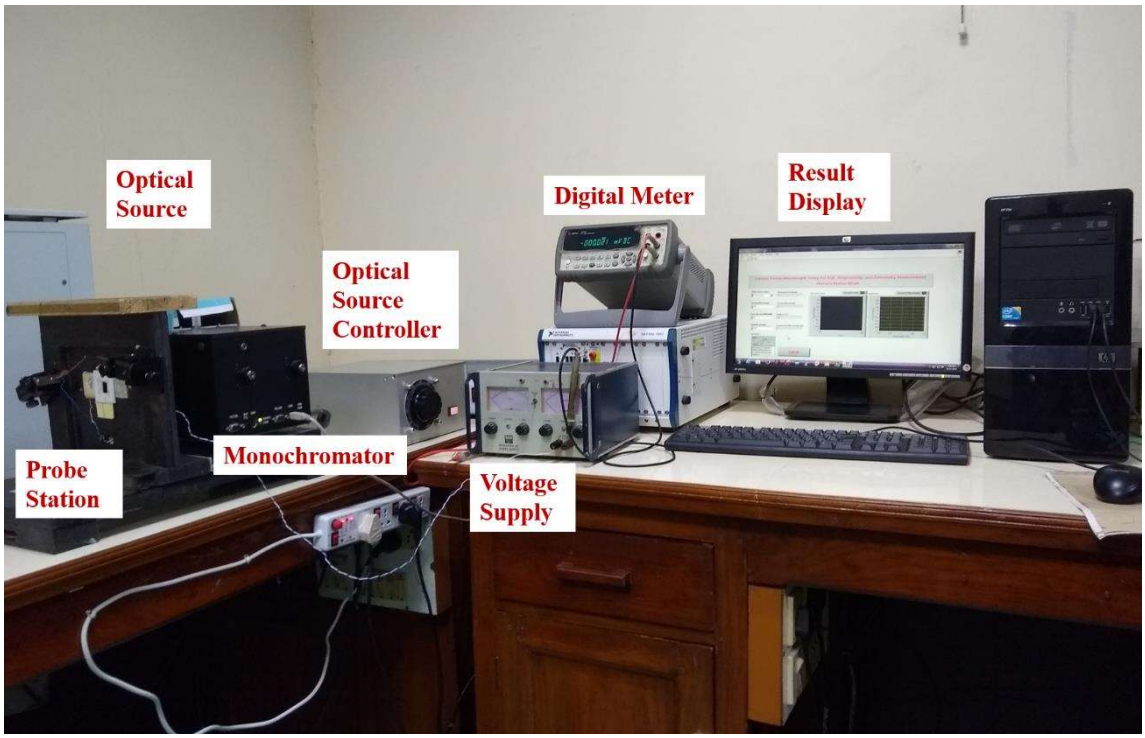


**Figure 1.16:** Experimental measurement setup for the photocurrent measurements.

*Time-Response Characteristics*: The response speed of any photodetector is expressed by the rise-time and fall-time of the photocurrent measured under the illumination by a pulsed optical signal of any finite duration. The duration over which the current magnitude is increased from 10% to 90% of the maximum amplitude under the illumination of the pulsed light is called the *rise-time"*. Similarly, the time duration during which the photocurrent value is reduced from 90% to 10% of the maximum value when the light is turned off is called *fall-time*. The smaller the values of rise time and fall time, the better will be the response speed of photodetectors.

## 1.5 Literature Review

The objective of the present thesis work is to investigate the photodetection properties of some $BiFeO_3$ (inorganic perovskite) and $CH_3NH_3PbI_3$ (hybrid halide perovskite) materials based thin film photodetectors. To outline the scope of the present thesis, it is important now to review some important state-of-the-art published works in the related area of research. The review of some general halide perovskite based optoelectronic devices will be discussed first. Then some important state-of-the-art research on $BiFeO_3$ and $CH_3NH_3PbI_3$ based photodetector devices will be discussed in the following subsections.

### 1.5.1 Perovskite Materials Based Devices: A General Review

Halide based organic-inorganic hybrid perovskites have been widely used for the photo absorber and visible light sensitizers since 2009. Kojima and co-workers have attempted to fabricate $MAPbX_3$ halide perovskite-based photovoltaic cells to obtain a high photovoltage of 1.0 V [37]. The photosensitivity of $CH_3NH_3PbI_3$ to the UV-visible spectrum of sunlight was investigated by Hu and co-workers [54]. Tunable optical properties of the $MAPbI_{3-x}Cl_x$ perovskite thin films were reported by Wang *et al.* [55]. They observed better performance in Au/perovskite and Ag/perovskite devices than Cu/perovskite and Al/perovskite devices over the 405-800 nm spectral range. Zhao *et al.* observed that narrow bandgap hybrid perovskites could be formed with the combination of halogen X ions [56]. Wang *et al.* and Xu *et al.* investigated the properties of the hybrid perovskites blended with Sn and Pb [57], [58]. Properties of Cs doped formamidinium lead iodide ($FAPbI_3$) hybrid perovskite was investigated by Liang *et al.* [59]. Dou. *et al.* [60] synthesized $CH_3NH_3PbI_{3-x}Cl_x$ by solution method for fabricating an inverted structure-based broadband photodetector using PEDOT: PSS and PCBM layers as the

HTL and ETL respectively. Guo *et al.* [61] observed responsivity of 7.85 A/W at solar-blind UV light (254 nm) and 14.5 A/W for white light in $MAPbI_{3-x}Cl_x$ perovskite thin films with a water-resistant polymer (CYTOP). Liu and co-workers fabricated a $CH_3NH_3PbI_3$ perovskite photodetector using $TiO_2$ as a compact layer and PCBM as ETL to demonstrate a high detectivity of $4x10^{12}$ Jones in 375- 800 nm spectral range [39]. Sutherland *et al.* [62] explored the material tailoring in perovskites for photodetector applications using $TiO_2$ and Spiro-OMeTAD as ETL and HTL, respectively. Xie *et al.* fabricated a $MAPbI_{3-x}Cl_x$/PEDOT: PSS based heterojunction broadband photodetector to demonstrate the maximum responsivity of $10^9$ A/W and detectivity of $10^{14}$ Jones over a wide range of 350-1100 nm at a low bias voltage of -0.5 V [63]. Tang *et al.* obtained a high detectivity of 1.1 $x10^{13}$ Jones and a fast response time of 2.2 µs in a $CH_3NH_3PbI_{3-x}Cl_x$ based photodetector with PEDOT: PSS as HTL and a blended mixture of 20 wt % PMMA and PCBM as ETL. They attributed the high performance to improved hole injection blocking by the PMMA and PCBM blended ETL [64]. The crystalline $CsPbBr_3$ perovskite was explored for photodetection applications by Dirin *et al.* [65]. They reported a high responsivity of 6 A/W at 550 nm under a bias voltage of -10 V. Maculan *et al.* [66] fabricated a single-crystalline $CH_3NH_3PbCl_3$ based visible-blend UV photodetector and measured the maximum responsivity of 0.05 A/W and detectivity 1.2 $x10^{12}$ Jones at 365 nm under -15 V bias voltage. Cao. *et al*. obtained a responsivity of 0.01 A/W at 450 nm in a $CH3NH_3PbBr_3/CH_3NH_3PbI_xBr_{3-x}$ heterojunction photodetector [67]. $C_sPbBr_3$ monolayer and multiple-layer based printable high-speed photodetectors were reported by Song *et al* [68]. They observed the responsivity of 0.64 A/W at 517 nm under -10 V bias voltage with a rise-time/fall-time of 19 µs/25 µs. Similarly, Li *et al.* [69] reported a CNT modified $CsPbBr_3$ based photodetector to demonstrate a high responsivity of 31.1 A/W at 517 nm wavelength under -10 V bias voltage with a rise-

time/fall-time of 17.8ms/14.7ms. Arquer *et al.* [70] reported a solution-processed perovskite with PbS quantum dots-based photodetector to achieve the maximum responsivity of 0.1 A/W at 975 nm and detectivity of $4x10^{12}$ Jones at 1240 nm under -1V bias voltage. Jarwal *et al.* [71] reported a maximum efficiency of 15.16% in $TiO_2$ nanorods based perovskite solar cells synthesized by solvothermal etching or $TiCl_4$ treatment process. Yu *et al.* [72] and Zheng *et al.* [73] studied ZnO and $TiO_2$ ETL based perovskite photodetectors to extend the spectral response towards a shorter wavelength or UV region. A $TiO_2$/Graphene/$MAPbI_3$ structure-based broadband self-powered photodetector operating in 260-900 nm was reported by Li *et al.* [74]. Pandey *et al.* reported a $BaTiO_3$/ZnO heterojunction-based UV-Vis photodetector [75]. $BaTiO_3$ perovskite was also explored for UV detection by Ma *et al.* [76]. Chen *et al.* [77] investigated the effect of the top layer on the photovoltaic properties of inorganic $BiFeO_3$ perovskite. Effect of white light on $BiFeO_3$/Nb: $SrTiO_3$ heterojunction with a large rectifying ratio of $10^4$ was investigated by Qu *et al.* [78]. Jo *et al.* [79] reported a dielectric constant of 405, dielectric-loss of 0.03% and leakage current density of $2.52 \times 10^{-7}$ A/cm$^2$ in the PZT/ $BiFeO_3$ thin film heterojunction.

Since the present thesis investigates the performance of some $BiFeO_3$ and $CH_3NH_3PbI_3$ based photodetectors, we will now review some important literature on the related devices in the following two subsections.

### 1.5.2 Review of Inorganic $BiFeO_3$ Perovskite Based Photodetectors

Both the Curie and Neel temperatures of the bismuth ferrite ($BiFeO_3$) material were reported to be above the room temperature by Wang *et al.* [80]. Using band structure modeling, $BiFeO_3$ was shown to possess both the direct and indirect bandgap properties by Clark and Robertson [28]. In 2009, Choi *et al.* [31] investigated the photovoltaic

properties of Au/$BiFeO_3$/Au diode. Yang *et al.* [81] obtained an external quantum efficiency (EQE) of 10% and open-circuit voltage of 0.8–0.9 V in a $BiFeO_3$ based solar cell. Zang *et al.* [82] reported a graphene/$BiFeO_3$/Pt heterojunction photodetector with a short circuit current density (Jsc) of 25 μA/$cm^2$ and open-circuit voltage of 0.44 V. Anshul *et al.* [83] fabricated a $BiFeO_3$ thin film photodetector grown on a patterned interdigitated electrode for visible light detection. The photovoltaic–pyroelectric coupled effect in $BiFeO_3$ based self-powered photodetector was investigated by Qi *et al* [84]. Luo *et al.* [85] investigated resistive switching in NiO/$BiFeO_3$ thin Film deposited on Pt/Ti/$SiO_2$/Si substrate. Chatterjee *et al.* [29] fabricated an intrinsic $BiFeO_3$ perovskite-based *p-i-n* heterojunction based photodetector. A $BiFeO_3$ perovskite-based *p-i-n* heterojunction based white light photodetector with a responsivity of 0.04 A/W was reported by Mondal *et al* [27]. However, $BiFeO_3$ has been little explored for photodetector applications. Thus, there is ample opportunity to explore the material for photodetection applications.

### 1.5.3 Review of Hybrid $CH_3NH_3PbI_3$ Perovskite Based Photodetectors

The first $CH_3NH_3PbI_3$ hybrid perovskite-based photodetector was reported by Hu *et al.* [54]. Lin *et al.* [86] demonstrated a $CH_3NH_3PbI_3$ perovskite-based self-biased IR-blind photodetector for visible light detection and imaging with the maximum detectivity of ~$10^{12}$ Jones at ~700 nm and rise-time/fall-time of 1.7 μs/1.0 μs. Fang *et al.* [87] fabricated a $CH_3NH_3PbI_3$ based photodetector with a responsivity of ~0.21 A/W at -2 V, detectivity of ~7.4 x $10^{12}$ Jones at -0.1 V, and fall time of 120 ns at 680 nm. Bao *et al.* [88] explored $CH_3NH_3PbI_3$ for fabricating a self-powered photodetector using Au nanowires based transparent electrodes to achieve a responsivity of ~0.32 A/W at 670 nm and rise-time/fall-time of 4.0 μs /3.3 μs. A high-performance self-powered photodetector with a responsivity of 0.29 A/W and detectivity of ~3.29 x$10^{12}$ Jones at 490 nm; and rise-

time/fall-time of 20 µs /17 µs was reported by Li *et al.* [89]. Wang *et al.* [90] used vapour-assisted multi-functional $CH_3NH_3PbI_3$ thin films for fabricating photodetectors exhibiting the maximum responsivity of 0.4 A/W and detectivity ~3 x$10^{12}$ Jones at -0.1 V bias voltage and 650 nm. Shen *et al.* integrated a $CH_3NH_3PbI_3$ layer with PDPPTDTPT polymer layer to fabricate a wideband photodetector for sensing light over the UV-NIR region and reported the maximum detectivity of ~$10^{11}$ Jones at -0.1 V bias and 900 nm [91]. Liu *et al.* [92] explored solution-processed $CH_3NH_3PbI_3$ and PbS quantum dots to fabricate a broadband photodetector which exhibited the maximum responsivity of ~0.3 A/W and detectivity ~1.2x $10^{13}$ Jones at 500 nm. Domanski *et al.* [93] analysed the interplay between photoconductivity and voltage-driven energy-level alignment of hybrid perovskite $CH_3NH_3PbI_3$ based low-voltage photodetector of responsivity ~208 A/ W at 500 nm and -0.6 V bias voltage, and rise-time/fall-time of <0.01 s. Dong *et al.* reported a $CH_3NH_3PbI_3$ nanocrystals-based photodetector to obtain a responsivity of ~242 A/W at 740 nm and -1 V bias voltage; and rise-time/fall-time of 10 µs/5.7 µs [94]. Zhou *et al.* [95] reported a self-powered, ultraviolet-visible photodetector based on heterojunction of $TiO_2$ nanorods and CH3NH3$PbI_3$. The fabricated photodetector showed good ultraviolet-visible photo-response characteristics with a responsivity of 0.26 A/W and 0.85 A/W at 364 nm and 494 nm, respectively. Hu *et al.* [96] fabricated a $CH_3NH_3PbI_3$ based flexible broadband photodetector and reported the highest responsivity of ~3.49 A/W at 365 nm and applied bias of -3 V. $CH_3NH_3PbI_3$/C8BTBT heterojunction based broadband photodetector was investigated by Tong *et al.* [97] and achieved a high $I_{light}/I_{dark}$ ratio of $2.4 \times 10^4$ and responsivity up to 24.8 A/W. A heterojunction based on $CH_3NH_3PbI_3$/ZnO nanorod arrays for broadband photodetector was also reported by Yu *et al.* [98]. They achieved the maximum responsivity of ~24.3 A/W, detectivity of ~3.56x $10^{14}$ Jones at 500 nm, and rise-time/fall-time of 0.7 s/0.6 s. Wang *et al.* [99] fabricated a

$CH_3NH_3PbI_3/C_{60}$ heterojunction-based photodetector to achieve a high EQE value of ~80% in the visible region (400 to 760 nm) with a low dark current density of ~0.6 nA/cm$^2$ and high detectivity ~2.7x10$^{13}$Jones. Wang *et al.* [100] reported an improvement in stability and performance of PCBM/$CH_3NH_3PbI_3$ heterojunction-based photodetector with a variation of PCBM thickness and obtained the maximum responsivity of 0.18 A/W at 365 nm with response time ~123 ms. Hu *et al.* [101] explored germanium/perovskite $CH_3NH_3PbI_3$ based heterostructure for broadband photodetection in the visible to infrared telecommunication band which showed the maximum responsivity of 1.4 A/W at 1550 nm and 228 A/W at 680 nm. Erkilic *et al.* [102] demonstrated large-area 2D perovskite $MAPbI_3/WS_2$ heterojunction-based photodetector by vapour phase selective growth method which exhibited the maximum responsivity of 43.6 A/W at 532 nm. Li *et al.* [103] investigated a perovskite $CH_3NH_3PbI_3$/CdS heterostructure based photodetector which showed the maximum responsivity of 0.43 A/W and detectivity of 2.3 × 10$^{11}$ Jones at 730 nm. Chaudhary *et al.* [104] investigated the effect of thickness on the performance of $CH_3NH_3PbI_3$ perovskite-based planar heterojunction photodiodes and obtained the maximum detectivity of 1.42 x 10$^{12}$ Jones for 450 nm of active layer thickness. Liu *et al.* [105] reported a large-area $CH_3NH_3PbI_3$/PMMA heterojunction based broadband photodetector with the maximum responsivity of 0.46 A/W, detectivity of 3.18×10$^{10}$ Jones and rise/fall times of 0.21/0.12s. Li *et al.* [106] fabricated a $CH_3NH_3PbI_3$/C8BTBT heterojunction based broadband photodetector by chemical vapour deposition method to demonstrate the maximum responsivity of 6.09 AW at 405 nm and rise-time/fall-time of 30/12 ms. Xiao *et al.* [107] reported a monolithic $CH_3NH_3PbI_3/PbI_2$ vertical heterostructure based flexible broadband photodetector which showed the maximum detectivity up to 1.66 × 10$^{12}$ Jones, responsivity of 4.79 A/ W and rise time of 16 ms at 375 nm illumination.

## 1.6 Major Observations from the Literature Survey

In this section, we have summarised the major observations derived from the literature survey as given in the following:

- Among various hybrid perovskites, $CH_3NH_3PbI_3$ perovskite is the most widely investigated material for photodetection applications due to its high carrier mobilities, modest band gap, good chemical solubility, long carrier lifetimes, simplified fabrication process, long exciton diffusion length, and low defect density in the energy band [35]-[38]. $CH_3NH_3PbI_3$ perovskite-based photodetector also has a low saturation current during operation [39], [40].
- $CH_3NH_3PbI_3$ perovskite has widely explored for solar cell applications [35], [38], [40], [44], [47], [48], [71]. Some works on $CH_3NH_3PbI_3$ based photodetectors have also been reported [34], [36], [39], [54]-[62]. However, there are ample opportunities for performance optimization through transport layer engineering of $CH_3NH_3PbI_3$ based photodetectors.
- The perovskite thin-film devices using inorganic $BiFeO_3$ perovskite are of great interest for electronic and optoelectronic applications due to as good chemical stability, a wide range of bandgap, eco-friendly, switchable rectifying behaviour and low-temperature fabrication processing [26]-[32]. However, only limited works have been reported on the $BiFeO_3$ based photodetectors [27], [29], [31], [81]-[85]. However, no significant works have been reported on $BiFeO_3$ based white light photodetectors.
- Several hybrid halide perovskite $CH_3NH_3PbI_3$ based heterojuction devices have photodetectors have been reported in the literature [27], [29], [31], [63],

[67], [75], [78], [95], [97]-[107]. However, no significant works have been reported on $CH_3NH_3PbI_3/BiFeO_3$ heterojunction photodetectors.

In brief, there are ample opportunities to explore both the hybrid halide perovskite $CH_3NH_3PbI_3$ and inorganic perovskite $BiFeO_3$ for photodetection applications. A lot of challenges still exist in the performance optimization of the above materials based photodetectors through device structure engineering, transport layer engineering and fabrication process engineering techniques.

## 1.7 Issues and Challenges in Perovskite Photodetectors

It is observed from the literature that inorganic/hybrid perovskite materials based electronic devices are conquering popularity due to their low cost and low-temperature fabrication processing. However, these materials have not been widely explored for optoelectronic applications. There are some obstacles for large scale fabrication of perovskite-based heterojunction optoelectronic devices. The major challenge in hybrid perovskite devices is to maintain the stability of electrical characteristics over a longer period. The perovskite material undergoes degradation due to moisture, temperature, and UV radiation. Several efforts have been made to enhance the chemical and phase stability, and toxicity of the hybrid perovskites. The hybrid perovskite $CH_3NH_3PbI_3$ is decomposed in $CH_3NH_3I^+$, hydrogen iodide, lead iodide in the presence of water. Thus, care has to be taken for fabricating $CH_3NH_3PbI_3$ based devices through solution processing. The correct selection of ETL/HTL material which has good compatibility with perovskite films such as protection of the inner organic layers from the air, favourable energy band alignment, and prevention of the recombination of charge carrier at electrode material interface can overcome the degradation of underneath perovskite film. Another major challenge in hybrid perovskite (active layer) based photodetectors is wideband photoresponse, which

limits the use of such detectors for practical spectrum selective applications. This drawback can be solved by using suitable optical filter layers as well as hole blocking layers with hybrid perovskite materials. On the other hand, the major challenge in inorganic perovskite $BiFeO_3$ is the growth of films, either the deposition parameters or targets can result in stoichiometry fluctuations and defects in $BiFeO_3$. The impurity defects in BFO will pin the domain wall and hinder the back witching of ferroelectric polarization, which deteriorate the performance of the device and this can be solved using the low-cost solid-state synthesis route with spin coating deposition process. The other challenge is the inefficient excitation of e–h pairs in ferroelectric inorganic perovskite $BiFeO_3$ can lead to a small photocurrent in the single inorganic perovskite-based device. To generate more e–h pairs, semiconductors layers such as ETL and HTL have to be introduced in a device.

## 1.8 Motivation and Problem Definition

As discussed above, inorganic/hybrid perovskite materials face many challenges related to their synthesis and fabrication of highly stable perovskite thin films for photodetection applications. Inorganic perovskite $BiFeO_3$ have relatively superior features over the other widely used inorganic perovskite $BaTiO_3$ and $PbTiO_3$ materials. Similarly, the hybrid perovskite $CH_3NH_3PbI_3$ possess relatively superior features over the other hybrid halide perovskite materials. That is why $BiFeO_3$ and $CH_3NH_3PbI_3$ are believed to be explored for photodetection applications. The objective of the present thesis work is to investigate the electrical and photodetection properties of some inorganic/hybrid perovskite thin film-based photodetector devices fabricated by spin-coating deposition techniques. Further, the improvement of electrical and photodetection performance characteristics using ZnO nanostructure materials for the ETL in the

photodetectors are also an area of interest to many researchers. Characterizations of $BiFeO_3$ and $CH_3NH_3PbI_3$ perovskite materials-based sol-gel derived thin films for photodetection applications could be of interest to many working in this area. Most interestingly, the $BiFeO_3/CH_3NH_3PbI_3$ inorganic-organic heterojunctions are also useful for photodetection applications.

## 1.9 Scope and Layout of the Thesis

The present thesis work deals with the fabrication and characterization of some inorganic/hybrid perovskite-based devices for photodetection applications. This thesis comprises five chapters including the present chapter. The remaining four chapters are briefly described as follows:

**Chapter-2** reports the fabrication and characterization of an inorganic perovskite $BiFeO_3$ based fast response white light photodetector. The device structure is ITO/ZnO (NPs)/ $BiFeO_3$ (NPs)/ PEDOT: PSS/Ag where the ITO (indium doped tin oxide) is used as the substrate, a layer of ZnO NPs is used for the ETL, $BiFeO_3$ (BFO) layer is used for the active layer of the device, the PEDOT: PSS (poly (3,4-ethylene dioxythiophene): polystyrene sulfonate) layer acts as the HTL and Ag film acts as metal electrode contact on the HTL of the device. ZnO nanoparticles are synthesized by the sol-gel process and the $BiFeO_3$ is synthesised by using the solid-state route. ZnO NPs, $BiFeO_3$ NPs and PEDOT: PSS polymer are deposited on the ITO substrate by the spin-coating method. The morphological, structural and optical characterizations of the thin films of $BiFeO_3$ NPs and ZnO NPs have been studied by the SEM images, XRD analysis, and UV-Vis spectrum, respectively. Finally, the photoresponse characteristics of the proposed ITO/ZnO NPs/BFO $NP_S$/PEDOT: PSS/Ag has been measured under dark and white light

illumination. The responsivity and external quantum efficiency of the proposed device have been measured over a broad spectrum of 400 to 750 nm.

**Chapter-3** introduces the fabrication and characterization of a hybrid perovskite $CH_3NH_3PbI_3$/ZnO heterostructure based UV-visible wideband photodetector. The proposed device structure is FTO/ZnO NPs/ $CH_3NH_3PbI_3$/ MoOx/Ag where the FTO (fluorine-doped tin oxide) is the substrate, the layer of ZnO NPs (nanoparticles) is used for the ETL, $CH_3NH_3PbI_3$ layer acts as the active layer, MoOx layer acts as the HTL and Ag film acts as contact electrode in the proposed photodetector device. The hybrid perovskite $CH_3NH_3PbI_3$ and ZnO NPs are synthesized using the sol-gel route. The morphological, and structural characteristics of the $CH_3NH_3PbI_3$ and ZnO NPs thin films are studied by the SEM images and XRD analysis, respectively, while the optical characteristics have been investigated by UV-Vis spectroscopy and photoluminescence (PL) spectroscopy. Finally, the responsivity and EQE characteristics of the proposed FTO/ZnO/$CH_3NH_3PbI_3$/MoOx/Ag photodetector have been measured over a broad spectrum of 350 to 700 nm.

**Chapter-4** reports the fabrication and characterization of an Ag/$CH_3NH_3PbI_3$/$BiFeO_3$/ITO structure-based heterojunction broadband photodiode where the ITO coated glass is used for the substrate, $CH_3NH_3PbI_3$/$BiFeO_3$ heterojunction is the main active region of the device and Ag is used for the metal contact electrode placed on the hybrid $CH_3NH_3PbI_3$ perovskite. The inorganic perovskite $BiFeO_3$ is synthesized by using the solid-state route while the hybrid perovskite $CH_3NH_3PbI_3$ is synthesized by using the sol-gel chemical route as considered in Chapter-2 and Chapter-3, respectively. The structural, morphological, and optical properties of hybrid perovskite $CH_3NH_3PbI_3$ and inorganic perovskite $BiFeO_3$ have been studied by XRD

analysis, SEM images, and UV-Vis spectroscopy, respectively. The responsivity and EQE characteristics have been studied over a broad spectrum of 400-900 nm. The proposed device is shown to have a dual-band detection feature due to the individual absorption characteristics of $BiFeO_3$ and $CH_3NH_3PbI_3$ perovskites used in the device.

Finally, **Chapter-5** summarizes the major objectives and concludes the major findings of the present thesis. This chapter also outlines some future scope of works related to this thesis.